AIAA JOURNAL
Vol. 49, No. 6, June 2011

Technical Notes

Direct Numerical Simulation Database for Impinging Shock Wave/Turbulent Boundary-Layer Interaction

Sergio Pirozzoli* and Matteo Bernardini†
University or Rome "La Sapienza," 00184 Rome, Italy

DOI: 10.2514/1.J050901

Nomenclature

H	=	shape factor, δ^*/θ
M	=	Mach number
Re	=	Reynolds number
u_τ	=	friction velocity
δ	=	99% velocity boundary-layer thickness
δ^*	=	displacement thickness
θ	=	momentum thickness
τ_w	=	wall shear stress
φ	=	incidence angle of shock generator

Subscripts

imp	=	shock impingement point
in	=	inflow properties
rec	=	recycling station
rms	=	root-mean-square value
0	=	properties at reference upstream station
1	=	properties past incident shock
∞	=	freestream properties

Superscripts

$+$	=	viscous units
$*$	=	interaction coordinates

Introduction

THE interactions of shock waves with turbulent boundary layers developing over solid surfaces (shock wave boundary-layer interactions, hereinafter referred to as SBLIs) have great technological interest in the aerospace industry as they frequently occur in high-speed air intakes, turbomachine cascades, helicopter blades, supersonic nozzles, and launch vehicles [1]. When a shock wave interacts with a boundary layer, its main effect is to cause a sudden retardation of the flow with subsequent thickening and, in many cases, separation of the boundary layer. These phenomena have a significant (typically negative) impact on the aerodynamic performance of aircraft through their influence on the global force coefficients. Furthermore, the low-frequency unsteadiness associated with intermittent flow separation can be the cause of strong buffeting of the aircraft structures, which may lead to failure due to structural fatigue or cause damage of payload.

Although SBLIs may occur in many different configurations, the focus is here on the canonical problem of an oblique shock wave in a supersonic stream impinging on a flat plate where a turbulent boundary layer is developing. For this type of interaction, a substantial body of work has been done over the years, including both experiments [2–5] and numerical simulations [6–10] to mention but a few recent contributions.

Regarding experiments, recent developments in high-speed particle image velocimetry (PIV) have allowed us to get insight into the unsteady features of SBLIs with high resolution both in space and time [4]. However, measurements in the very near-wall region are still difficult, and access to the full field of velocity gradients is far from simple. This represents a serious drawback for the development of accurate turbulence models, which requires access to high-order statistics, such as Reynolds stress budgets, that cannot be obtained experimentally. Furthermore, one of the outcomes of the recent European research program UFAST[‡] (unsteady effects of shock-wave-induced interaction) was that experimental results are critically affected by the (necessarily finite) spanwise size of the wind tunnel, and side effects may also be present for relatively weak SBLIs.

Large-eddy simulations (LES) and direct numerical simulations (DNS) of SBLIs have appeared only in relatively recent times, owing to the substantial computational effort involved in the simulation of complex wall-bounded flows and difficulties encountered to control the numerical dissipation of shock-capturing algorithms. Early numerical simulations [6,7] have given insight into aspects of the SBLI physics that were not entirely clear at that time. In particular, it was found that, even in the absence of mean flow separation, scattered spots of instantaneously reversed flow are present in the interaction zone, which are associated with unsteady release of vortical structures into the mainstream and with the formation of a mixing layer, which persists well downstream of the nominal shock impingement position. Furthermore, it was shown that the amplification of turbulence is not directly related to the interacting shock but rather to the enhanced turbulent activity associated with the development of the mixing layer. More recent studies [8,9] have also revealed the ability of numerical simulations (both DNS and LES) to predict the low-frequency motion of the shock, previously observed in experiments. Such information cannot be gained from Reynolds-averaged Navier–Stokes (RANS) calculations.

In the present Note, we describe a numerical DNS database that was developed using a large computational domain with low-dissipative spatial discretization, and that is intended to serve as a reference for the development of advanced turbulence models (for both RANS and LES) capable to account for nonequilibrium effects. For that purpose, statistical quantities and raw flow sample data are made publicly available on a web site, which will allow other investigators to access any property of interest. In the following, we briefly describe the numerical algorithm and present a limited number of results, comparing them with recent experimental data.

Numerical Methodology

The flow solver used to generate the database was extensively used for the analysis of many compressible wall-bounded flows, also in the presence of interacting shocks [11]. In the current version of the code, the convective fluxes are discretized by means of a hybrid conservative scheme. The switch from central- to fifth-order

Received 3 September 2010; revision received 13 December 2010; accepted for publication 14 December 2010.

*Assistant Professor, Department of Mechanical and Aerospace Engineering, Via Eudossiana 18.

†Research Assistant, Department of Mechanical and Aerospace Engineering, Via Eudossiana 18.

‡Data available at http://www.ufast.gda.pl [retrieved 14 Feb. 2011].

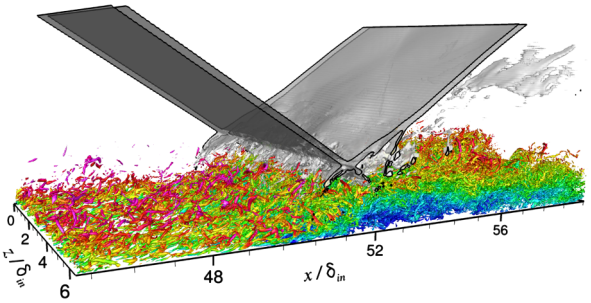

Fig. 1 Flow organization in impinging shock/boundary-layer interaction.

weighted-essentially nonoscillatory (WENO) discretization is controlled by a modified Ducros sensor,

$$\Theta = \frac{(\nabla \cdot u)^2}{(\nabla \cdot u)^2 + (\nabla \times u)^2 + (u_\infty/\delta_{\text{in}})^2}, \qquad 0 \le \Theta \le 1 \qquad (1)$$

which becomes large when the local dilatation is comparable to the vorticity magnitude and larger than a typical large-scale velocity gradient. The shock-capturing algorithm is activated whenever the sensor becomes larger than a suitable threshold to selectively add numerical dissipation only in the immediate proximity of shock waves (see Fig. 1). Specifically, for the purpose of hybridization, critical points (here defined as those where $\Theta > 0.15$) are preliminarily marked and then padded with four points on both sides to ensure that the stencil of the underlying nondissipative scheme does not cross shocked zones [12].

Improved numerical stability for the central discretization in smooth parts of the flow is achieved by splitting the convective derivatives as [13]

$$\frac{\partial \rho u_j \varphi}{\partial x_j} = \frac{1}{2}\frac{\partial \rho u_j \varphi}{\partial x_j} + \frac{1}{2}u_j \frac{\partial \rho \varphi}{\partial x_j} + \frac{1}{2}\rho\varphi \frac{\partial u_j}{\partial x_j} \qquad (2)$$

where φ stands for any transported quantity, being unity for the continuity equation, u_i $(i = 1, 2, 3)$ stands for the momentum equation, and $H = \gamma/(\gamma - 1)p/\rho + u_k u_k/2$ stands for the total energy equation. The derivative operators are then discretized with eighth-order finite difference formulas using a locally conservative formulation [14], which guarantees global conservation of mass, momentum, and total energy through the telescopic property and simplifies hybridization with the WENO algorithm. It is important to note that the use of the convective split form (2) guarantees strong numerical stability without reverting to any stabilization expedient, such as upwinding or filtering.

The diffusive terms in the Navier–Stokes equations are also approximated with eighth-order central differences after being expanded to Laplacian form to guarantee finite molecular dissipation at all resolved wavelengths. Time advancement is performed by means of a standard four-stage fourth-order explicit Runge–Kutta algorithm.

Purely nonreflecting characteristic conditions are used at the outflow and at the top boundary away from the incoming shock, where the inviscid Rankine–Hugoniot jump conditions are locally imposed instead, to mimic the effect of a shock generator. Unsteady characteristic boundary conditions [15] are specified at the bottom no-slip wall, the wall temperature being set to the adiabatic value for the upstream boundary layer. The inlet turbulence is enforced using an extension of the recycling/rescaling procedure to compressible flows [16], whereby staggering in the spanwise direction is used to minimize spurious flow periodicity (see [17] for a full description). As customary in DNS and LES, periodicity in the spanwise direction is assumed. A computational analysis of the effect of the presence of sidewalls in strong SBLIs has recently been reported by [18].

Description of Numerical Database

The flow conditions for the DNS have been chosen to be similar to those of the experiments of Piponniau et al. [3] (see also Dupont et al. [2] and Souverein et al. [5]), where the interacting shock is produced by deflection of the supersonic stream from a wedge-shaped shock generator. Specifically, the freestream Mach number is $M_\infty = 2.28$, and the incidence angle of the shock generator is $\varphi = 8°$. However, due to the huge computational resources required by reproduction of the full-scale experimental conditions, the Reynolds number (being $Re_{\theta_0} \approx 5100$ in the experiment) is reduced here to $Re_{\theta_0} \approx 2300$.

The computational domain used for the DNS has an overall size of

$$L_x \times L_y \times L_z = 80.58\delta_{\text{in}} \times 12.89\delta_{\text{in}} \times 6.47\delta_{\text{in}}$$

(where δ_{in} is the boundary-layer thickness at the inflow) in the streamwise, wall-normal, and spanwise directions, respectively. It is discretized with a grid consisting of $3841 \times 344 \times 261$ points and split into 64 subzones for convenient multiblock parallelization. The grid points are uniformly spaced in the streamwise and spanwise directions, and they are clustered in the wall-normal direction according to a hyperbolic sine mapping up to $y = 2.69\delta_{\text{in}}$ and then uniformly spaced up to the top boundary upon preliminary smoothing to guarantee preservation of the formal order of accuracy in the presence of grid stretching. For that purpose, metrics are evaluated with the same finite difference formulas as the spatial derivatives [19]. In terms of wall units (evaluated upstream of the interaction zone), the streamwise grid spacing is $\Delta x_0^+ \approx 5.6$, and the spanwise spacing is $\Delta z_0^+ = 6.6$. The spacing in the wall-normal direction (Δy_0^+) ranges from 0.93 at the wall to 15.2 at the top of the computational box. The ratio of the effective mesh spacing $\Delta = (\Delta x \cdot \Delta y \cdot \Delta z)^{1/3}$ to the local Kolmogorov length scale η is checked a posteriori to be less than five throughout the interaction zone, which

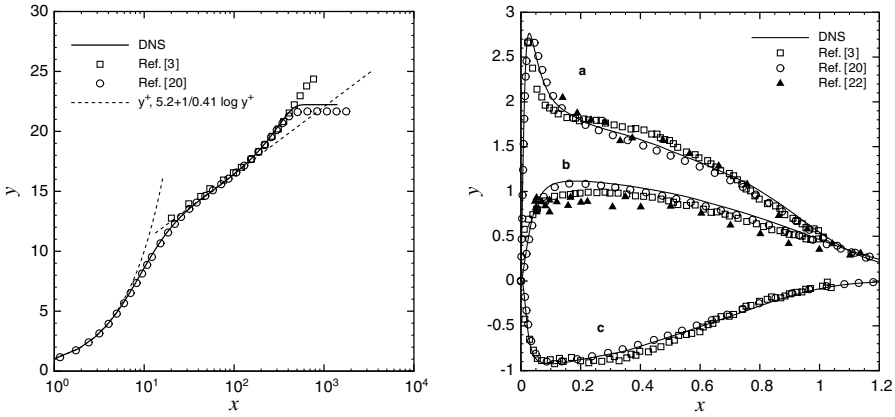

a) **b)**

Fig. 2 At reference station: a) mean streamwise velocity and b) density-scaled velocity fluctuations intensities.

Table 1 Incoming boundary-layer properties[a]

Parameter	Value
M	2.28
$\delta_0^*/\delta_{\text{in}}$	0.497
$\theta_0/\delta_{\text{in}}$	0.140
$Re_{\theta 0}$	2344
$Re_{\tau 0}$	466
H_0	3.55
C_{f0}	$2.56 \cdot 10^{-3}$

[a] Data are taken at the reference station ($x_o = 43.6\delta_{\text{in}}$) corresponding to $x^* = -1.93$ in interaction coordinates.

indicates that all the relevant scales of turbulent motion are adequately resolved. The recycling station is located at a distance of $x_{\text{rec}} = 42.98\delta_{\text{in}}$ from the inlet, which is sufficient to guarantee proper streamwise decorrelation of the boundary-layer statistics, thus preventing any spurious low-frequency motions associated with the recycling procedure [20]. The nominal shock impingement point is set at $x_{\text{imp}} = 53.72\delta_{\text{in}}$.

The calculation has been advanced in time until statistical steadiness is achieved at the nondimensional time $t = 283.5\delta_{\text{in}}/u_\infty$, and samples of the full three-dimensional field have been collected at time intervals of $0.493\delta_{\text{in}}/u_\infty$, up to the time $t = 701.9\delta_{\text{in}}/u_\infty$, for a total of 848 flow samples.

The instantaneous flow organization can be appreciated from inspection of Fig. 1, where the shock system is identified through the modified Ducros sensor of Eq. (1), and vortical structures through isosurfaces of the swirling strength [21]. The figure highlights the three-dimensional nature of the interaction zone: numerous elongated vortex tubes resembling those observed in incompressible boundary-layer DNS are found both in the upstream boundary layer and past the interacting shock. Note that the threshold value used for the shock sensor guarantees that numerical dissipation is confined in the close proximity of shock waves, whereas the wall layer is essentially depleted of critical zones, which implies that turbulence structures are not contaminated by spurious energy drain.

Computational Results

A preliminary assessment of the present DNS is reported in Fig. 2, where the mean velocity and the Reynolds stresses are shown at the reference station upstream of the interaction ($x_{\text{ref}} = 43.6\delta_{\text{in}}$). The structure of the incoming flow is compared with laser Doppler velocimetry (LDV) and PIV measurements [3,22] (both at $M \approx 2.3$, $Re_\tau \approx 1100$) and with incompressible DNS data at $Re_\tau = 445$ [20]. The mean velocity profile well conforms to the log law upon van Driest scaling, which also leads to collapse with reference low-speed data at comparable friction Reynolds number. The density-scaled Reynolds stresses also exhibit close similarities with the incompressible distributions, and satisfactory collapse is also obtained with experiments for the streamwise component and the shear stress. Some discrepancy is observed instead for the wall-normal velocity fluctuations, which are larger in DNS. However, underestimation of the wall-normal velocity component is a typical

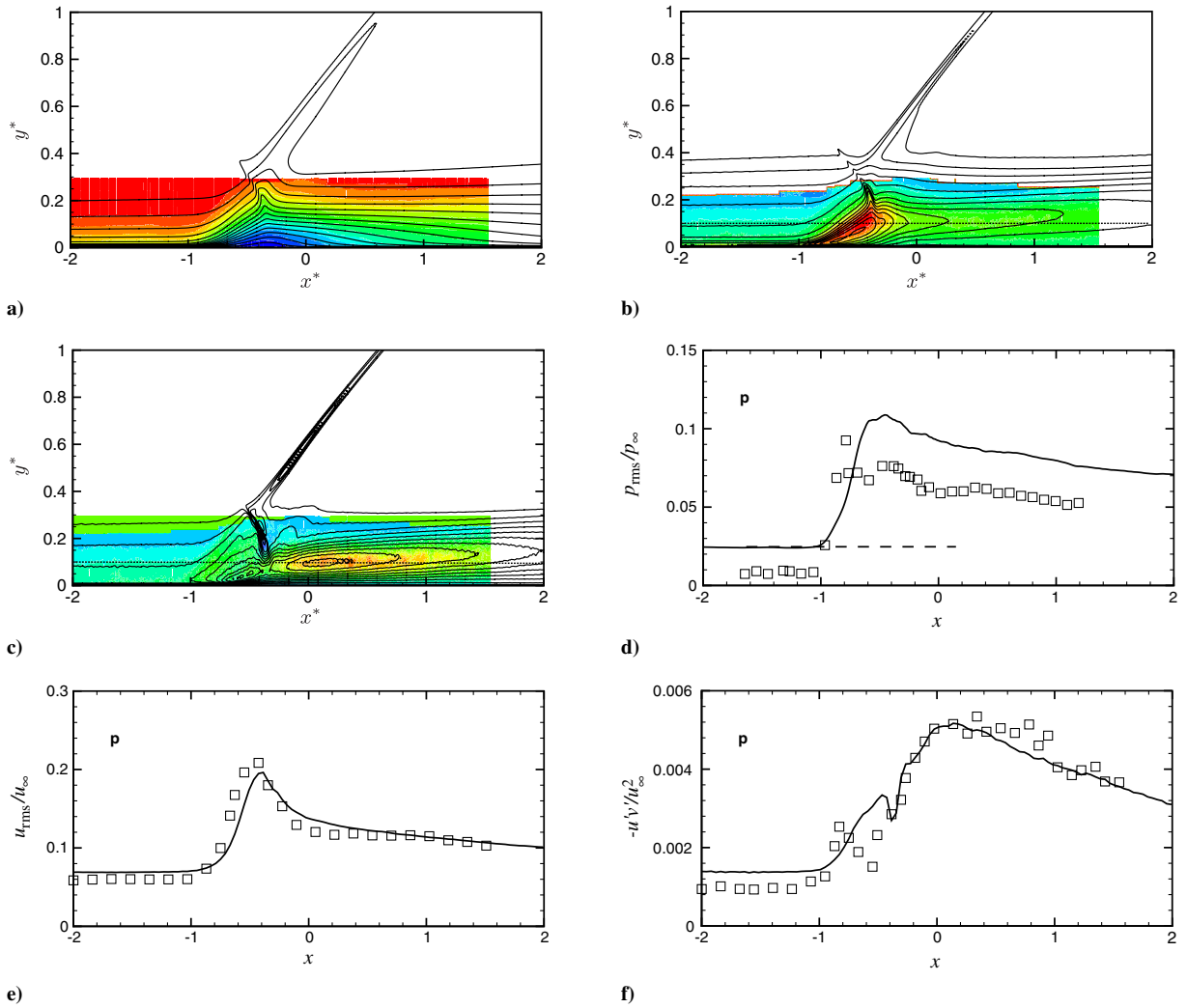

Fig. 3 Flow properties across the interaction (lines: present DNS; flooded contours and □: [3]): a) $\bar{u}/u_\infty$, b) u_{rms}/u_∞, c) $-\overline{u'v'}/u_\infty^2$, d) p_{rms}/p_∞ at the wall, e) u_{rms}/u_∞ at $y^* = 0.1$, and f) $-\overline{u'v'}/u_\infty^2$ at $y^* = 0.1$.

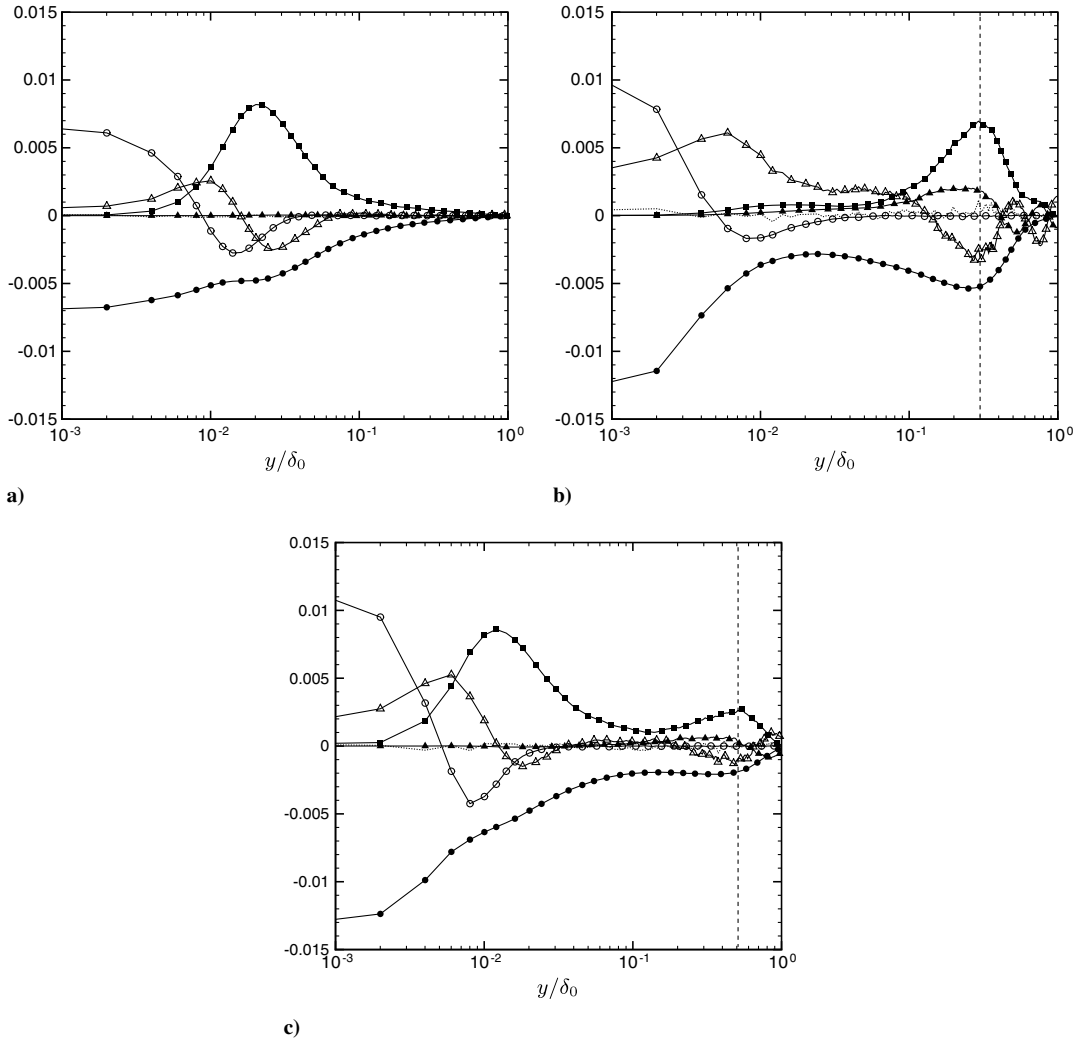

Fig. 4 Turbulence kinetic energy balance at a) $x^* = -1.93$, b) $x^* = -0.05$, and c) $x^* = 2.1$ (▲: advection; △: turbulent transport; ■: production; ○: viscous diffusion; ●: viscous dissipation).

feature of both PIV and LDV [22,23]. Looking at the global properties of the upstream boundary layer (reported in Table 1), we also note that (consistently with the difference in the Reynolds number) the skin friction coefficient is larger than the experimental value, $C_f \approx 2.1 \cdot 10^{-3}$ [3,22].

A comparison of the velocity statistics across the interaction zone is reported in Fig. 3 together with the distribution of the root-mean-square wall pressure. Note that, since DNS and experiments are performed at different Re_τ, a convenient way of comparing the data [24] is to rescale the coordinate axes with respect to an interaction length scale, here defined as the distance between the nominal impingement point of the incoming shock and the apparent origin of the reflected shock. It turns out that, for the present DNS, the ratio of the interaction length scale to the upstream boundary-layer thickness is $L/\delta_0 = 2.89$, whereas in the experiments of Piponniau et al. [3], $L/\delta_0 \approx 4.18$. This significant discrepancy in the overall size of the interaction zone is likely to be the result of the difference in the Reynolds number. Indeed, as pointed out by Dupont et al. [2], direct proportionality exists between the interaction size L/δ_0 and the nondimensional incident shock strength, defined as $(p_1 - p_\infty)/(2\tau_{w0})$. This implies that larger interactions zones should be expected at larger Reynolds numbers. For the present DNS data, we have $(p_1 - p_\infty)/(2\tau_{w0}) \approx 33$ (this parameter is about 40 in the experiment), for which the data reported by Dupont et al. [2] (see their Fig. 7) actually support $L/\delta_0 \approx 3$.

Having introduced scaled interaction coordinates, $x^* = (x - x_{\text{imp}})/L$ and $y^* = y/L$, to compensate Reynolds number differences, Fig. 3 shows that the structure of the interaction zone is well recovered. Specifically, the thickening of the boundary layer is well reproduced, as well as the amplification of the Reynolds stresses past the interaction zone associated with the shedding of vortices. On the other hand, significant discrepancy is observed in the distribution of the root-mean-square wall pressure, which is substantially lower in the experiment but in agreement with the p_{rms} estimates for a zero-pressure-gradient boundary layer [25]. As reported in the study of Dupont et al. [2], where the focus was on the low-frequency motions, such differences are due to the underestimation of p_{rms} caused by the low-cutoff frequency of the pressure transducers, which did not allow those authors to explore the high-frequency pressure fluctuations associated with fine-grained turbulence.

Useful information for RANS modelers comes from analysis of the terms in the budget of the turbulence kinetic energy ($k = 1/2\widetilde{u_i'' u_i''}$) equation, which in the compressible case can be cast as

$$\underbrace{-\frac{\partial \bar{\rho}\tilde{u}_j k}{\partial x_j}}_{C} \underbrace{-\frac{\partial}{\partial x_j}\left[\frac{1}{2}\bar{\rho}\,\widetilde{u_i'' u_i'' u_j''} + \overline{p' u_j''}\right]}_{T} \underbrace{-\bar{\rho}\,\widetilde{u_i'' u_j''}\frac{\partial \tilde{u}_i}{\partial x_j}}_{P} \underbrace{+\frac{\partial}{\partial x_j}(\overline{\sigma_{ij}'' u_i''})}_{V} \underbrace{-\overline{\sigma_{ij}'}\frac{\partial u_i''}{\partial x_j}}_{D} \underbrace{+\overline{p'\frac{\partial u_i''}{\partial x_i}} + \overline{u_i''}\left(\frac{\partial \bar{\sigma}_{ij}}{\partial x_j} - \frac{\partial \bar{p}}{\partial x_i}\right)}_{K} = 0 \tag{3}$$

including the contributions of mean advection C, turbulent and pressure transport T, production by mean velocity gradient P, viscous diffusion V, and viscous dissipation D, respectively. Pressure–dilatation correlations and mass diffusion effects are incorporated in the term K. The most significant terms for the k budget are reported in Fig. 4 at three representative stations ($x^* = -1.93$, -0.05, and 2.1), normalized by $\delta_0/\rho_\infty u_\infty^3$. Note that the sum of the budget is indicated with a dotted line in the figure, and the vertical dashed lines indicate the local position of the mixing layer midline. The upstream budget is typical of a canonical boundary layer, being dominated by the balance between production and dissipation in a large part of the boundary layer, except in the proximity of the wall, where turbulent transport and viscous diffusion are significant. A different behavior is observed at $x^* = -0.05$, where maximum production is attained well away from the wall, owing to the lift up of vortical structures in the mixing layer, and the advection term becomes significant, contributing to balance production. Partial recovery of an equilibrium state is observed at $x^* = 2.1$, where the wall-detached production peak is still visible but lower than the inner peak. Note that all terms (except C, which is computed at run time) have been estimated using the stored flow samples, and no filter has been used to smooth the profiles.

Conclusions

A novel DNS database for canonical impinging shock/turbulent boundary-layer interaction has been presented. The underlying numerical algorithm is based on a high-order central energy-consistent discretization of the convective derivatives that does not require upwinding or filtering to guarantee nonlinear numerical stability. The use of a modified Ducros sensor guarantees that the strict amount of numerical dissipation necessary to inhibit Gibbs oscillations is added only in the immediate proximity of shock waves, and the smooth turbulence structures are not contaminated by spurious energy drain. The main flow properties, in terms of velocity and pressure field statistics, have been compared with existing high-quality experimental data. Even though a one-to-one comparison is not possible, owing to limitations in the attainable Reynolds number, the global prediction of the flow structure is in good agreement with experiments when obvious differences in the overall size of the interaction zone are suitably compensated. It is believed that the present database fills in an existing gap, and it may represent a reliable resource for the validation of RANS- and LES-based prediction methods, also allowing to probe quantities that are difficult to measure in experiments, such as the fluctuating pressure, for which a substantial scatter is noticed in the literature. Additional efforts are being made to further extend the duration of the calculation to accurately access information on the low-frequency dynamics of the interaction. Both raw data in the form of three-dimensional flow samples and precomputed flow statistics are available, together with full supporting documentation.[§]

Acknowledgments

The support of the Consorzio Interuniversitario per le Applicazioni di Supercalcolo Per Università e Ricerca (CASPUR)[¶] through the 2010 grant titled, "Analysis of low-frequency motions in shock wave/boundary-layer interactions," is gratefully acknowledged. The authors wish to thank J. P. Dussauge for providing the experimental data reported in the Note.

References

[1] Délery, J., and Dussauge, J. P., "Some Physical Aspects of Shock Wave/Boundary Layer Interactions," *Shock Waves*, Vol. 19, No. 6, 2009, pp. 453–468. doi:10.1007/s00193-009-0220-z

[2] Dupont, P., Haddad, C., and Debiève, J. F., "Space and Time Organization in a Shock-Induced Separated Boundary Layer," *Journal of Fluid Mechanics*, Vol. 559, 2006, pp. 255–277. doi:10.1017/S0022112006000267

[3] Piponniau, S., Dussauge, J. P., Debiève, J. F., and Dupont, P., "A Simple Model for Low-Frequency Unsteadiness in Shock-Induced Separation," *Journal of Fluid Mechanics*, Vol. 629, 2009, pp. 87–108. doi:10.1017/S0022112009006417

[4] Humble, R. A., Scarano, F., and Van Oudheusden, B. W., "Particle Image Velocimetry Measurements of a Shock Wave/Turbulent Boundary Layer Interaction," *Experiments in Fluids*, Vol. 43, Nos. 2–3, 2007, pp. 173–183. doi:10.1007/s00348-007-0337-8

[5] Souverein, L. J., Dupont, P., Debiève, J. F., Dussauge, J. P., van Oudheusden, B. W., and Scarano, F., "Effect of Interaction Strength on Unsteadiness in Turbulent Shock-Wave-Induced Separations," *AIAA Journal*, Vol. 48, No. 7, 2010, pp. 1480–1493. doi:10.2514/1.J050093

[6] Garnier, E., Sagaut, P., and Deville, M., "Large-Eddy Simulation of Shock/Boundary-Layer Interaction," *AIAA Journal*, Vol. 40, No. 10, 2002, pp. 1935–1944. doi:10.2514/2.1552

[7] Pirozzoli, S., and Grasso, F., "Direct Numerical Simulation of Impinging Shock Wave/Turbulent Boundary Layer Interaction at $M = 2.25$," *Physics of Fluids*, Vol. 18, No. 6, 2006, Paper 065113. doi:10.1063/1.2216989

[8] Priebe, S., Wu, M., and Martin, M. P., "Direct Numerical Simulation of a Reflected Shock Wave/Turbulent Boundary Layer Interaction," *AIAA Journal*, Vol. 47, No. 5, 2009, p. 1173–1184. doi:10.2514/1.38821

[9] Touber, E., and Sandham, N. D., "Large-Eddy Simulation of Low-Frequency Unsteadiness in a Turbulent Shock-Induced Separation Bubble," *Theoretical and Computational Fluid Dynamics*, Vol. 23, No. 2, 2009, pp. 79–107. doi:10.1007/s00162-009-0103-z

[10] Morgan, B., Kawai, S., and Lele, S. K., AIAA Paper 2010-4467, 2010.

[11] Bernardini, M., Pirozzoli, S., and Grasso, F., "The Wall Pressure Signature of Transonic Shock/Boundary Layer Interaction," *Journal of Fluid Mechanics*, 2011 (in press).

[12] Visbal, M. R., and Gaitonde, D. V., "Shock Capturing Using Compact-Differencing-Based Methods," AIAA Paper 2005-1265, 2005.

[13] Blaisdell, G. A., Spyropoulos, E. T., and Qin, J., "The Effect of the Formulation of Non-Linear Terms on Aliasing Errors in Spectral Methods," *Applied Numerical Mathematics*, Vol. 21, No. 3, 1996, pp. 207–219. doi:10.1016/0168-9274(96)00005-0

[14] Pirozzoli, S., "Generalized Conservative Approximations of Split Convective Derivative Operators," *Journal of Computational Physics*, Vol. 229, No. 19, 2010, pp. 7180–7190. doi:10.1016/j.jcp.2010.06.006

[15] Poinsot, T. S., and Lele, S. K., "Boundary Conditions for Direct Simulations of Compressible Viscous Flows," *Journal of Computational Physics*, Vol. 101, No. 1, 1992, pp. 104–129. doi:10.1016/0021-9991(92)90046-2

[16] Sagaut, P., Garnier, E., Tromeur, E., Larchevêque, L., and Labourasse, E., "Turbulent Inflow Conditions for Large-Eddy Simulation of Compressible Wall-Bounded Flows," *AIAA Journal*, Vol. 42, No. 3, 2004, pp. 469–477. doi:10.2514/1.3461

[17] Pirozzoli, S., Bernardini, M., and Grasso, F., "Direct Numerical Simulation of Transonic Shock/Boundary Layer Interaction Under Conditions of Incipient Separation," *Journal of Fluid Mechanics*, Vol. 657, 2010, pp. 361–393. doi:10.1017/S0022112010001710

[18] Garnier, E., "Stimulated Detached Eddy Simulation of the Three-Dimensional Shock/Boundary Layer Interaction," *Shock Waves*, Vol. 19, No. 6, 2009, pp. 479–486. doi:10.1007/s00193-009-0233-7

[19] Visbal, M. R., and Gaitonde, D. V., "On the Use of Higher-Order Finite-Difference Schemes on Curvilinear and Deforming Meshes," *Journal of Computational Physics*, Vol. 181, No. 1, 2002, pp. 155–185. doi:10.1006/jcph.2002.7117

[20] Simens, M. P., Jiménez, J., Hoyas, S., and Mizuno, Y., "A High-Resolution Code for a Turbulent Boundary Layers," *Journal of Computational Physics*, Vol. 228, No. 11, 2009, pp. 4218–4231. doi:10.1016/j.jcp.2009.02.031

[21] Zhou, J., Adrian, R., Balachandar, S., and Kendall, T., "Mechanisms for Generating Coherent Packets of Hairpin Vortices in Channel Flow," *Journal of Fluid Mechanics*, Vol. 387, No. , 1999, pp. 353–396. doi:10.1017/S002211209900467X

[22] Elena, M., and Lacharme, J. P., "Experimental Study of a Supersonic Turbulent Boundary Layer Using a Laser Doppler Anemometer,"

[§]Data available at http://grassopc.dma.uniroma1.it/osbli/ [retrieved 14 Feb. 2011].

[¶]Data available at http://www.caspur.it [retrieved 14 Feb. 2011].

Journal of Theoretical and Applied Mechanics, Vol. 7, No. 2, 1988, pp. 175–190.

[23] Souverein, L. J., "On the Scaling and Unsteadiness of Shock Induced Separation," Ph.D. Thesis, Faculty of Aerospace Engineering, Delft Univ. of Technology, Delft, The Netherlands, 2010, http://repository.tudelft.nl/view/ir/uuid%3A23aa05e7-0762-4d13-bbe9-adccfc7e505a [retrieved 14 Feb. 2011].

[24] Délery, J., and Marvin, J. G., "Shock-Wave Boundary Layer Interactions," AGARDograph 280, 1986.

[25] Farabee, T., and Casarella, M. J., "Spectral Features of Wall Pressure Fluctuations Beneath Turbulent Boundary Layers," *Physics of Fluids*, Vol. 3, No. 10, 1991, pp. 2410–2420. doi:10.1063/1.858179

P. Tucker
Associate Editor